Instability and Diapycnal Momentum Transport in a Double-Diffusive, Stratified Shear Layer

WILLIAM D. SMYTH AND SATOSHI KIMURA

College of Oceanic and Atmospheric Sciences, Oregon State University, Corvallis, Oregon

(Manuscript received 18 November 2005, in final form 1 September 2006)

ABSTRACT

The linear stability of a double-diffusively stratified, inflectional shear flow is investigated. Double-diffusive stratification has little effect on shear instability except when the density ratio R_ρ is close to unity. Double-diffusive instabilities have significant growth rates and can represent the fastest-growing mode even in the presence of inflectionally unstable shear with a low Richardson number. In the linear regime, background shear has no effect on double-diffusive modes except to select the orientation of the wave vector. The converse is not true: double-diffusive modes modify the mean shear via momentum fluxes. The momentum flux driven by salt sheets is parameterized in terms of a Schmidt number (ratio of eddy viscosity to saline diffusivity) Sc_s. In the oceanic parameter regime, Sc_s is less than unity and can be approximated as $\mathrm{Sc}_s = 0.08\ \ln[\mathrm{R}_\rho/(\mathrm{R}_\rho - 1)]$. Enhanced molecular dissipation by unstable motions is quantified in terms of the dissipation ratio Γ, and the results are compared with observations. Corresponding results are given for diffusive convection in an inflectional shear flow, though linear theory is expected to give a less accurate description of this mechanism.

1. Introduction

Thermohaline stratification is double-diffusively unstable for nearly half of the ocean interior (You 2002). The instability often results in layering, which may occur through two mechanisms that have been seen as distinct, though their relationship is poorly understood. When temperature and salinity vary only in the vertical, the fluid becomes organized into staircases of vigorously convecting layers separated by thin interfaces (Radko 2003). When temperature and salinity vary in the horizontal, buoyancy fluxes may drive interleaving motions that have the potential to effect significant lateral transport between water masses. Effects of shear (i.e., vertically sheared horizontal currents) may be important in both scenarios. In the interleaving case, shear is clearly present between adjacent intruding layers (Mueller et al. 2007). In a staircase, shear is not intrinsic, but the ubiquitous presence of gravity waves in the ocean means that such layers will be subjected to shear nonetheless (e.g., Kunze 1994).

Corresponding author address: William D. Smyth, College of Oceanic and Atmospheric Sciences, Oregon State University, Corvallis, OR 97331-5503.
E-mail: smyth@coas.oregonstate.edu

DOI: 10.1175/JPO3070.1

While the last few decades have seen many studies of double-diffusive instability, the effects of shear on those instabilities have received relatively little attention. Linden (1974) showed both theoretically and experimentally that a uniform shear favors convection rolls whose axes are parallel to the background flow. Analogous results have been found for ordinary convection in the presence of shear (Deardorff 1965). Thangham et al. (1984) conducted detailed numerical studies of shear effects, but excluded inflectional profiles (i.e., flows in which shear is vertically localized, our main focus here). Kunze (1990, 1994) considered equilibration of finite-amplitude salt fingers in shear, including the oceanically important case of inertially rotating shear. Wells et al. (2001) conducted laboratory experiments on salt fingers in a vertically periodic shear and showed how the strength of the salt fingers adjusted to create an equilibrium state. Other investigators have looked into the spontaneous generation of shear by divergent double-diffusive fluxes (Paparella and Spiegel 1999; Stern 1969; Holyer 1981).

The ability of double-diffusive motions to flux horizontal momentum in the vertical has been addressed experimentally by Ruddick (1985) and Ruddick et al. (1989), and observationally by Padman (1994). Double-diffusive momentum fluxes are thought to be crucial in

determining the vertical scales of thermohaline interleaving layers (Toole and Georgi 1981).

Here, we consider instability in a vertically localized layer where diffusively unstable stratification and shear coincide. The inflectional nature of the imposed shear yields the possibility of Kelvin–Helmholtz (KH) instability independent of double diffusion. We delineate regions of parameter space in which each class of instability is likely to dominate, and also consider the effects of double-diffusive stratification on KH instability. We examine the effect that the finite vertical extent of the stratified layer has on the characteristics of double-diffusive instability relative to the previously studied case of uniform gradients.

One of the most useful outcomes that any study of ocean mixing can produce is a prediction of the fluxes due to the mixing process in question. Predictions of double-diffusive fluxes are needed for the interpretation of observational data (e.g., Gregg and Sanford 1987; Padman and Dillon 1987; Hebert 1988; Rudels et al. 1999; Timmermans et al. 2003) and for models ranging from global simulations (Zhang et al. 1998; Merryfield et al. 1999) to small-scale processes studies (e.g., Walsh and Ruddick 1998; Merryfield 2000). In the linear (small amplitude) limit, fluxes grow exponentially. In reality, this exponential growth is arrested with the onset of nonlinear effects, which generally lead the flow to a turbulent state. Fluxes occurring at finite amplitude cannot be predicted from linear theory. The situation becomes more encouraging if one considers ratios of fluxes. As a linear eigenmode grows exponentially in time, any flux ratio will remain constant. One therefore knows the value of the flux ratio at the onset of nonlinear effects, and this provides a plausible estimate of the flux ratio that will pertain in fully nonlinear flow. For example, the ratio of thermal to saline buoyancy fluxes in exponentially growing salt fingers is a simple function of R_ρ that agrees well with the flux ratio in the fully nonlinear state (e.g., Schmitt 1979; Kunze 2003).

Here, we attempt to parameterize momentum fluxes in terms of the better understood buoyancy fluxes, using flux ratios in the form of Prandtl and Schmidt numbers. Results are in reasonable agreement with available laboratory and observational evidence, but provide a more comprehensive view of the parameter dependences of these flux ratios.

The dissipation ratio Γ is frequently used to characterize mixing processes (e.g., McDougall and Ruddick 1992; Ruddick et al. 1997; St. Laurent and Schmitt 1999). Like the Prandtl and Schmidt numbers, Γ is constant in the linear regime. We compute Γ for small-amplitude salt sheets in shear, and find that the results compare reasonably well to observations of finite-amplitude salt fingering in weakly sheared flow (St. Laurent and Schmitt 1999).

Our primary focus is on the salt fingering regime, in which warm, salty fluid overlies cooler, fresher fluid. In the opposite scenario, linear theory predicts oscillatory diffusive convection. Diffusive convection as it occurs in the laboratory and the ocean is an intrinsically finite-amplitude phenomenon and is poorly modeled by its linear counterpart. Nevertheless, the linear dynamics are not without interest and are included here for completeness.

Our basic tool is linear stability analysis, whose application is described in section 2. The description of the results begins in section 3 with an overview of the main classes of unstable modes that may occur in a diffusively unstable, sheared flow: salt fingers, salt sheets, KH instabilities, and diffusive convection. We discuss the physics of each and define Schmidt and Prandtl numbers with which to describe the momentum fluxes. In section 4, we look at the effects of double-diffusive stratification on KH instabilities. Background shear does not affect double-diffusive instabilities directly (except to select their orientation), but the instabilities may affect the background flow by transporting momentum in the vertical. This process, and its parameterization, are the subjects of section 5. We then give an equivalent (though less detailed) discussion for diffusive convection in section 6. In section 7, we delineate the regions of parameter space in which each of these classes of instabilities is expected to dominate. Conclusions are given in section 8.

2. Methodology

a. The eigenvalue problem for linear normal modes

We assume that density is a linear function of temperature and salinity and neglect inertial effects of density variations in accordance with the Boussinesq approximation. The velocity field $\mathbf{u}(x, y, z, t) = \{u, v, w\}$ is measured in a nonrotating, Cartesian coordinate system $\{x, y, z\}$. The resulting field equations are

$$\frac{D\mathbf{u}}{Dt} = -\nabla\pi + b\hat{k} + \nu\nabla^2\mathbf{u}, \tag{1}$$

$$\nabla \cdot \mathbf{u} = 0, \tag{2}$$

$$\frac{Db_T}{Dt} = \kappa_T\nabla^2 b_T, \tag{3}$$

$$\frac{Db_S}{Dt} = \kappa_S\nabla^2 b_S, \quad \text{and} \tag{4}$$

$$b = b_T + b_S. \tag{5}$$

TABLE 1. Glossary of symbols.

Symbol	Definition
$\mathbf{u}(x, y, z, t)$	Velocity, $\{u, v, w\}$
$\mathbf{u}'(x, y, z, t)$	Velocity perturbation, $\{u', v', w'\}$
$U(z)$	Background velocity profile
U_{z0}	Central background shear
$b_T(x, y, z, t)$	Thermal buoyancy
$b'_T(x, y, z, t)$	Thermal buoyancy perturbation
$B_T(z)$	Background thermal buoyancy profile
B_{Tz0}	Central thermal buoyancy gradient
$b_S(x, y, z, t)$	Saline buoyancy
$b'_S(x, y, z, t)$	Saline buoyancy perturbation
$B_S(z)$	Background saline buoyancy profile
B_{Sz0}	Central total buoyancy gradient
B_{z0}	Central background buoyancy gradient
$\pi(x, y, z, t)$	Scaled pressure
$\Pi(z)$	Background pressure profile
$\pi'(x, y, z, t)$	Pressure perturbation
σ	Growth rate
k	Streamwise wavenumber
l	Spanwise wavenumber
$\tilde{k}$	Magnitude of wave vector
ν	Molecular viscosity
κ_T	Molecular thermal diffusivity
κ_S	Molecular saline diffusivity
h	Half thickness of layer
u_0	Half velocity change across layer
R_ρ	Density ratio: $-B_{Tz}/B_{Sz}$
Pr	Molecular Prandtl number: ν/κ_T
Sc	Molecular Schmidt number: ν/κ_S
τ	Diffusivity ratio: κ_S/κ_T
Re	Reynolds number: $u_0 h/\nu$
Gr	Grashof number: $B_{z0}h^4/\nu\kappa_T$
Ri_b	Bulk Richardson number: $\mathrm{Gr}/\mathrm{PrRe}^2$
γ_s	Salt finger buoyancy flux ratio
γ_d	Diffusive convection buoyancy flux ratio
ν_s	Salt finger viscosity
Pr_s	Salt sheet Prandtl number: Viscosity/thermal diffusivity
Pr_d	Diffusive convection Prandtl number
Sc_s	Salt finger Schmidt number: Momentum/saline diffusivity
Sc_d	Diffusive convection Schmidt number

The variable π represents the pressure scaled by the uniform characteristic density ρ_0, and $\hat{k}$ is the vertical unit vector. Buoyancy is defined as $b = -g(\rho - \rho_0)/\rho_0$, where g is the acceleration due to gravity. Buoyancy is the sum of a thermal component b_T and a saline component b_S. Kinematic viscosity and thermal and saline diffusivities are represented by ν, κ_T, and κ_S, respectively. Boundary conditions are periodic in the horizontal and flux free at $z = 0$ and $z = H$. Table 1 lists all symbols used in this paper.

The velocity, buoyancy, and pressure terms are separated into two parts, a background profile and a perturbation:

$$\mathbf{u}(x, y, z, t) = U(z)\hat{i} + \varepsilon \boldsymbol{u}'(x, y, z, t), \tag{6}$$

$$b_T(x, y, z, t) = B_T(z) + \varepsilon b'_T(x, y, z, t), \tag{7}$$

$$b_S(x, y, z, t) = B_S(z) + \varepsilon b'_S(x, y, z, t), \quad \text{and} \tag{8}$$

$$\pi(x, y, z, t) = \Pi(x, y, z, t) + \varepsilon \pi'(x, y, z, t). \tag{9}$$

We substitute (6)–(9) into (1)–(4) and then collect the $O(\varepsilon)$ terms. The perturbations are assumed to take the normal mode form:

$$w'(x, y, z, t) = \hat{w}(z)e^{\sigma t + i(kx + ly)} + \text{c.c.}, \tag{10}$$

where k and l are wavenumbers in streamwise and spanwise directions, respectively, and σ is the growth rate of the perturbation. Substituting these perturbations into the $O(\varepsilon)$ equations gives

$$\sigma\hat{u} = -ikU\hat{u} - \hat{w}U_z - ik\hat{\pi} + \nu\tilde{\nabla}^2\hat{u}, \tag{11}$$

$$\sigma\hat{v} = -ikU\hat{v} - il\hat{\pi} + \nu\tilde{\nabla}^2\hat{v}, \tag{12}$$

$$\sigma\hat{w} = -ikU\hat{w} - \hat{\pi}_z + \hat{b} + \nu\tilde{\nabla}^2\hat{w}, \tag{13}$$

$$0 = i(k\hat{u} + l\hat{v}) + \hat{w}_z, \tag{14}$$

$$\sigma\hat{b}_T = -ikU\hat{b}_T - \hat{w}B_{Tz} + \kappa_T\tilde{\nabla}^2\hat{b}_T, \tag{15}$$

$$\sigma\hat{b}_S = -ikU\hat{b}_S - \hat{w}B_{Sz} + \kappa_s\tilde{\nabla}^2\hat{b}_S, \quad \text{and} \tag{16}$$

$$\hat{b} = \hat{b}_T + \hat{b}_S, \tag{17}$$

where the subscript z indicates the derivative, $\tilde{\nabla}^2 = d^2/dz^2 - \tilde{k}^2$ and $\tilde{k}^2 = k^2 + l^2$. Eliminating $\hat{\pi}$ from (11)–(14), we obtain

$$\sigma\tilde{\nabla}^2\hat{w} = -ikU\tilde{\nabla}^2\hat{w} + ik\hat{w}U_{zz} + \nu\tilde{\nabla}^4\hat{w} - \tilde{k}^2\hat{b}. \tag{18}$$

Equations (15)–(18) form a closed, generalized, differential eigenvalue problem whose eigenvalue is σ and whose eigenvector is the concatenation of $\{\hat{w}, \hat{b}_T, \hat{b}_S\}$. The horizontal velocities and the pressure may then be obtained separately if needed.

The background profiles appearing in (11)–(18) are chosen to describe a stratified shear layer:

$$U = u_0 \tanh\frac{z}{h}, \tag{19}$$

$$B_{Tz} = \frac{R_\rho B_{z0}}{R_\rho - 1}\operatorname{sech}^2\frac{z}{h}, \quad \text{and} \tag{20}$$

$$B_{Sz} = \frac{-B_{z0}}{R_\rho - 1}\operatorname{sech}^2\frac{z}{h}. \tag{21}$$

Here, u_0 is the half velocity change across a layer of half depth h, B_{z0} is the maximum background buoyancy gradient (or squared buoyancy frequency), and $R_\rho = -B_{Tz}/B_{Sz}$ is the density ratio.

In the interleaving case, the assumption that shear varies vertically on the same scale as stratification is reasonable. If shear is imposed by an internal wave field, however, it is likely that the vertical scales will be very different. If thermohaline properties vary on a much smaller scale than velocity, there exists the potential for other classes of shear instability besides KH. If the shear field is aligned so that maximum shear coincides with a stratified interface, the result may be Holmboe instability (e.g., Smyth and Winters 2003). On the other hand, if the shear maximum is located between adjacent stratified layers, Taylor instability may result (e.g., Lee and Caulfield 2001). These will be the subject of a future publication.

b. Nondimensionalization

We nondimensionalize the problem using length scale h and time scale h^2/κ_T. This nondimensionalization introduces four dimensionless parameters: the molecular Prandtl number $\mathrm{Pr} = \nu/\kappa_T$, the diffusivity ratio $\tau = \kappa_S/\kappa_T$, the Reynolds number $\mathrm{Re} = u_0 h/\nu$, and the Grashof number[1] $\mathrm{Gr} = B_{z0}h^4/\nu\kappa_T$. The latter is just the additive inverse of the Rayleigh number and as such is positive in statically stable stratification. It is also a scaled version of the buoyancy gradient B_{z0}, which is equal to the squared Brunt–Väisälä frequency.

The equations needed for the analyses to follow become

$$\sigma\hat{u} = -ikU\hat{u} - \hat{w}U_z - ik\hat{\pi} + \mathrm{Pr}\tilde{\nabla}^2\hat{u}, \tag{22}$$

$$\sigma\tilde{\nabla}^2\hat{w} = -ikU\tilde{\nabla}^2\hat{w} + ik\hat{w}U_{zz} + \mathrm{Pr}\tilde{\nabla}^4\hat{w} - \tilde{k}^2\hat{b}, \tag{23}$$

$$\sigma\hat{b}_T = -\hat{w}B_{Tz} - ikU\hat{b}_T + \tilde{\nabla}^2\hat{b}_T, \quad \text{and} \tag{24}$$

$$\sigma\hat{b}_S = -\hat{w}B_{Sz} - ikU\hat{b}_S + \tau\tilde{\nabla}^2\hat{b}_S, \tag{25}$$

with background profiles

$$U = \mathrm{RePr}\tanh z, \tag{26}$$

$$B_{Tz} = \frac{R_\rho \mathrm{GrPr}}{R_\rho - 1}\mathrm{sech}^2 z, \quad \text{and} \tag{27}$$

$$B_{Sz} = \frac{-\mathrm{GrPr}}{R_\rho - 1}\mathrm{sech}^2 z. \tag{28}$$

In (22)–(28) and hereinafter unless otherwise noted, all quantities are dimensionless. For the computations described here, boundaries are located at $z = \pm 4$.

c. Numerical methods

The Fourier–Galerkin method is used to discretize the z dependence:

$$\{\hat{w}(z), \hat{b}_T(z), \hat{b}_S(z)\} = \sum_{n=1}^{N}\{\hat{w}_n, \hat{b}_{T_n}, \hat{b}_{S_n}\}f_n(z) \quad \text{and} \tag{29}$$

$$\{\hat{u}(z), \hat{v}(z), \hat{\pi}(z)\} = \sum_{n=1}^{N}\{\hat{u}_n, \hat{v}_n, \hat{\pi}_n\}g_n(z), \tag{30}$$

where

$$f_n(z) = \sin\frac{n\pi(z + H/2)}{H} \quad \text{and}$$

$$g_n(z) = \cos\frac{n\pi(z + H/2)}{H}. \tag{31}$$

The nondimensional domain height H is here set equal to 8. The inner product operator of any two functions $a(z)$ and $b(z)$ is defined by

$$\langle a(z)b(z)\rangle = \frac{2}{H}\int_0^H a(z)b(z)\,dz, \tag{32}$$

so that

$$\langle f_m(z)f_n(z)\rangle = \delta_{mn} \quad \text{and}$$

$$\langle g_m(z)g_n(z)\rangle = \delta_{mn}(1 + \delta_{m0}). \tag{33}$$

Equations (23)–(25) become

$$\begin{aligned}
\sigma\langle f_m\tilde{\nabla}^2 f_n\rangle\hat{w}_n &= (-ik\langle f_m U\tilde{\nabla}^2 f_n\rangle + ik\langle f_m U_{zz} f_n\rangle + \mathrm{Pr}\langle f_m\tilde{\nabla}^4 f_n\rangle)\hat{w}_n - \tilde{k}^2\langle f_m f_n\rangle\hat{b}_{Tn} - \tilde{k}^2\langle f_m f_n\rangle\hat{b}_{Sn},\\
\sigma\langle f_m f_n\rangle\hat{b}_{Tn} &= -\langle f_m B_{Tz} f_n\rangle\hat{w}_n - ik\langle f_m U f_n\rangle\hat{b}_{Tn} + \langle f_m\tilde{\nabla}^2 f_n\rangle\hat{b}_{Tn}, \quad \text{and}\\
\sigma\langle f_m f_n\rangle\hat{b}_{Sn} &= -\langle f_m B_{Sz} f_n\rangle\hat{w}_n - ik\langle f_m U f_n\rangle\hat{b}_{Sn} + \tau\langle f_m\tilde{\nabla}^2 f_n\rangle\hat{b}_{Sn}.
\end{aligned}$$

This is a generalized algebraic eigenvalue problem whose eigenvalue is σ and whose eigenvector is the concatenation of $\{\hat{w}_n, \hat{b}_{Tn}, \hat{b}_{Sn}\}$. Convergence requires up to 192 Fourier modes for boundaries located at $z = \pm 4$.

d. Parameter values

The molecular Prandtl number and the diffusivity ratio have the values $\mathrm{Pr} = 7$ and $\tau = 10^{-2}$, appropriate for

[1] We use the term somewhat loosely, as the buoyancy gradient in Gr contains a contribution from a second scalar (salinity) in addition to the one whose diffusivity appears in the denominator (temperature).

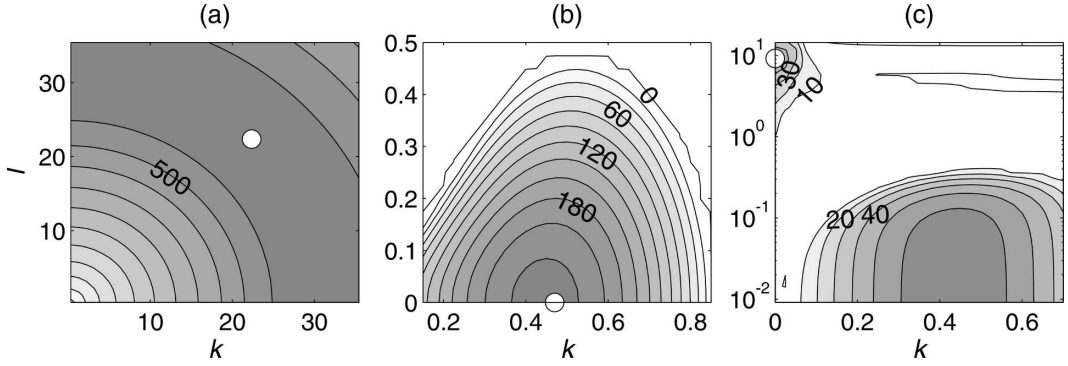

FIG. 1. The real part of the dispersion relation $\sigma_r(k, l)$ for three illustrative cases: (a) pure salt fingering: Re = 0, Gr = 10^6, $R_\rho = 1.6$; (b) pure KH: Re = 300, $\mathrm{Ri}_b = 0.1$, $R_\rho = 100$; and (c) KH and salt sheets: Re = 100, $\mathrm{Ri}_b = 0.1$, Gr = 7000, $R_\rho = 1.6$. Bullets indicate points for which flux profiles are shown in Fig. 2.

seawater. We also define the molecular Schmidt number, $\mathrm{Sc} = \mathrm{Pr}/\tau = 700$.

Here Gr is assumed to be positive, indicating stable stratification. Observations in a thermohaline staircase east of Barbados, summarized by Kunze (2003), suggest values in the range from 10^8 to 2×10^9; depending on how one relates h to the thickness of a double-diffusive layer.

Double-diffusive instability requires $(\mathrm{Pr} + \tau)/(\mathrm{Pr} + 1) < R_\rho < \tau^{-1}$ (or $0.876 < R_\rho < 100$ for the present parameter values) and is strongest when R_ρ is near unity. The Barbados observations yielded a typical value of 1.6. Here, we consider a range of values from 0.9 to 100.

The Reynolds number obtained from the Barbados observations is in the range 10^3–10^4. Values used here will range from 0, in the limit of no shear, to 10^8. The latter may exist in thin, strongly sheared layers not resolved in measurements.

Another parameter of interest is the bulk Richardson number, $\mathrm{Ri}_b = \mathrm{Gr}/(\mathrm{PrRe}^2)$. This is the minimum value of the gradient Richardson number, occurring at $z = 0$. Bulk Richardson number $\mathrm{Ri}_b < 1/4$ is the standard criterion for KH instability (Miles 1961; Howard 1961).

3. Overview of instabilities

In the absence of shear, double-diffusive instability creates convection rolls (and other planforms; e.g., Schmitt 1994) whose orientation is not determined, that is, the growth rate depends on the magnitude of the wave vector but not on its direction (Fig. 1a). In the absence of double-diffusive instability, inflectional shear may create dynamic instability, which for this flow configuration is KH instability. Unlike double-diffusive instability, KH instability is strongly directional, with wave vectors oriented parallel to the background shear flow growing most rapidly in accordance with Squire's theorem (Yih 1955). These modes have $l = 0$, and we refer to them as *transverse*. Of these, the mode with nondimensional wave vector near one-half (or wavelength about 7 times the thickness of the shear layer) grow the fastest (Fig. 1b).

Double-diffusive instability becomes directional in the presence of shear, with wave vectors oriented at right angles to the mean flow growing fastest. These modes have $k = 0$, and are referred to here as *longitudinal*. In accordance with Squire's theorem, longitudinal modes are unaffected by the background shear, a property we will explore in detail in section 5. Figure 1c shows a case in which both salt fingers and KH modes are unstable. The KH modes are strongest near $k = 0.45$, $l = 0$, as is true in ordinary stratification (e.g., Hazel 1972). Salt fingers, instead of being nondirectional as in Fig. 1a, are strongly damped except near $k = 0$ (upper-left corner of Fig. 1c). This causes the instability to take the form of longitudinal convection rolls, or *salt sheets*.

Diffusive convection cases are not included in Fig. 1 because their dispersion relations are qualitatively similar to the salt sheet case (Fig. 1c). The difference is that, rather than being stationary, modes are oscillatory with frequencies often far in excess of the growth rate.

Salt fingers grow because the positive buoyancy flux due to salinity advection outweighs the negative buoyancy flux due to thermal advection (Fig. 2a). Unlike salt fingers growing on uniform background gradients (e.g., Stern 1960; Baines and Gill 1969), motions are concentrated in a thin layer where background gradients are largest. (Note that the vertical extent included in Fig. 2a is much less than that of the domain.) The amplitudes of the fluxes are arbitrary in the linear regime, but their ratio is not. The flux ratio

$$\gamma_s = -\overline{b_T' w'}/\overline{b_S' w'} \tag{34}$$

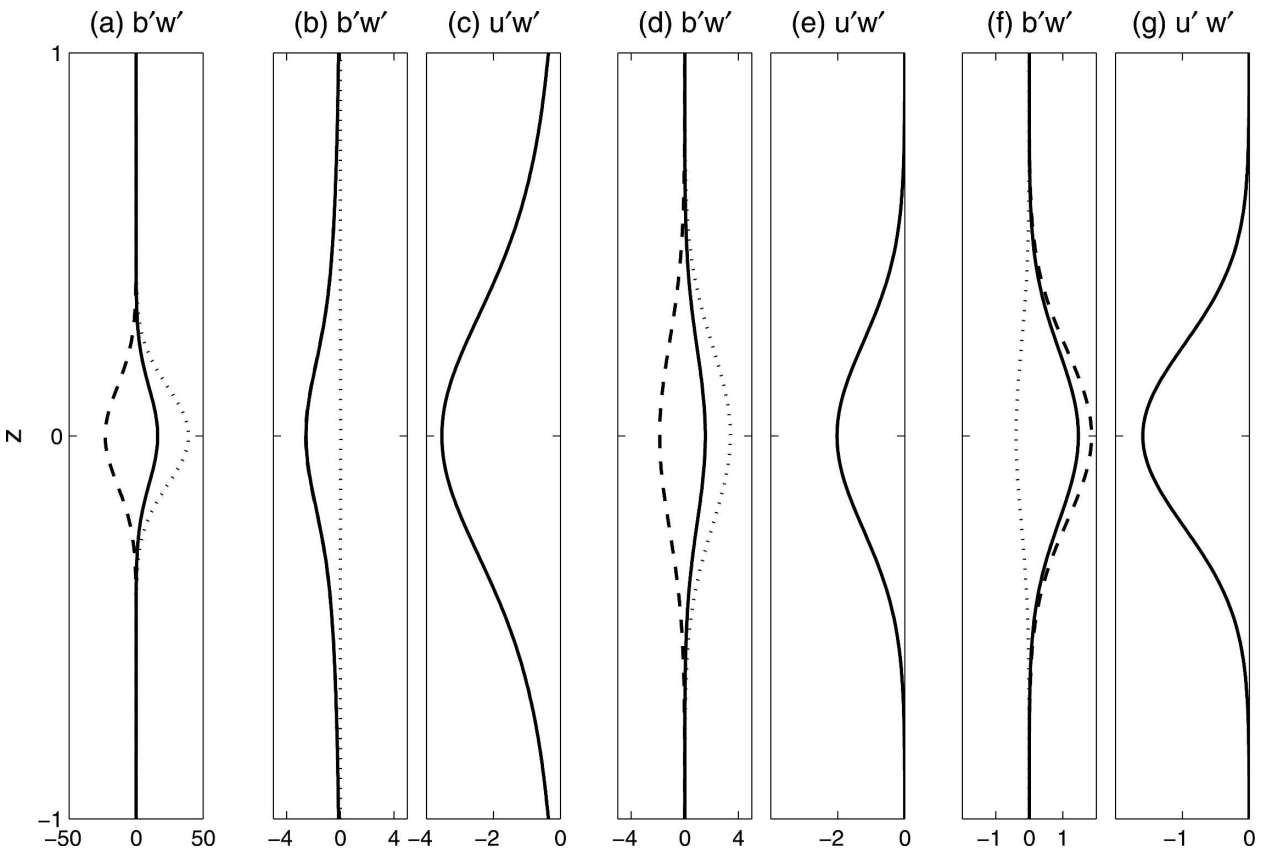

FIG. 2. Vertical fluxes of buoyancy and velocity for the three illustrative cases shown by bullets in Fig. 1, plus an example of sheared diffusive convection. (a) Pure salt fingering: Re = 0, Gr = 10^6, $R_\rho = 1.6$, $k = 22.36$, $l = 22.36$ (bullet in Fig. 1a). The velocity flux is not shown as it is identically zero. (b), (c) Pure KH: Re = 300, $\mathrm{Ri}_b = 0.1$, $R_\rho = 100$, $k = 0.47$, $l = 0$ (bullet in Fig. 1b). (d), (e) Sheared salt fingers: Re = 100, $\mathrm{Ri}_b = 0.1$, Gr = 7000, $R_\rho = 1.6$, $k = 0$, $l = 9.15$ (bullet in Fig. 1c). (f), (g) Sheared diffusive convection: Re = 100, $\mathrm{Ri}_b = 0.1$, Gr = 7000, $R_\rho = 0.96$, $k = 0$, $l = 9.15$. (a), (b), (d), (f) Buoyancy fluxes: total (solid), thermal (dashed), and saline (dotted). All buoyancy fluxes have been divided by 1000 for plotting convenience. (c), (e), (g) Velocity flux.

has the value 0.59 for this example. This value agrees well with measurements of salt fingers in laboratory and numerical experiments (Kunze 2003) and in the ocean (Schmitt 2003), despite having been derived from linear theory. This flux ratio also obtains in the vastly different parameter regime of sugar–salt fingers (Schmitt 1979).

The KH instability grows because the velocity flux (Fig. 2c) acts to reduce the background shear and thus draws energy from the mean flow into the perturbation. Because the stratification is almost purely thermal in this example, the same is true of the buoyancy flux (Fig. 2b). In fact, the flux ratio for this case is 93. This is similar to the value of the density ratio $R_\rho = 100$, indicating that the difference in the diffusivities of the two scalars plays no significant role in the dynamics, consistent with the fact that the mechanism of KH instability is essentially inviscid.

Salt sheets, like salt fingers, grow because of the dominance of the positive buoyancy flux due to salinity (Fig. 2d). For this example, $\gamma_s = 0.55$. In addition, convective motions within the salt sheets tilt against the shear, so that the velocity flux (Fig. 2e) draws energy from the mean flow to the perturbation. It is important to recognize that this energy transfer only amplifies motions in the x direction, and thus does not supply energy to the salt sheets per se. In fact, the background flow has no effect whatsoever on the salt sheet instability, in accordance with Squire's theorem.

The momentum and buoyancy fluxes may be expressed in terms of effective diffusivities via the usual flux-gradient formalism. The ratio of momentum to thermal diffusivity, here called the salt sheet Prandtl number Pr_s has the value 0.19, while the Schmidt number Sc_s, the ratio of momentum to saline diffusivity, is 0.07.

Diffusive convection is an oscillatory instability driven by the dominance of the positive thermal buoyancy flux over the negative saline buoyancy flux (Fig. 2f). The finite-amplitude expression of diffusive con-

vection is a *nonoscillatory* convective layering, suggesting a qualitative change in the physics between the small- and large-amplitude regimes, so that results from linear theory must be interpreted with caution. The flux ratio is defined oppositely to that for salt fingers:

$$\gamma_d = -\overline{b_S' w'}/\overline{b_T' w'}, \tag{35}$$

and has the value 0.21 for this example. Like salt sheets, sheared diffusive convection generates a vertical transport of momentum (Fig. 2f) via longitudinal convection cells. In contrast with the salt sheet case, momentum diffusivities are larger than scalar diffusivities. For the example shown in Figs. 2e,f, the Prandtl number of the diffusive convection is $\mathrm{Pr}_d = 1.46$ and the Schmidt number is $\mathrm{Sc}_d = 7.07$.

In subsequent sections, we will explore in detail the relationships between sheared, double-diffusive flow profiles and the instabilities they generate.

4. How are KH billows affected by double-diffusively unstable stratification?

For most oceanographic parameter values, diffusively unstable stratification has a negligible effect on KH instability. While this result is not obvious a priori, it is not surprising as the KH instability mechanism is inviscid. An exception occurs where $R_\rho \sim 1$. There, double-diffusive instability becomes so strong that, even when damped by shear, it overwhelms shear instability. (In this case the longitudinal salt sheet instability, being free of the damping effect of shear, is the dominant mode. Growth rates of salt sheets and KH billows are compared explicitly in section 7.)

An example is given in Fig. 3, which shows growth rate as a function of R_ρ and k for purely transverse modes with shear strong enough that the Richardson number is subcritical ($\mathrm{Ri}_b = 0.14$). The black contour signifies $\sigma_i = 0$; modes to the right of that contour are oscillatory. The white, dotted contour indicates the fastest-growing mode (FGM) at each R_ρ. For $R_\rho > 1.6$, the FGM is stationary and has wavenumbers near 0.45, as is characteristic of KH instability (Hazel 1972). At wavenumbers smaller than this fastest-growing KH mode, growth rates are independent of R_ρ for all R_ρ, as indicated by vertical contours.

In ordinary stratification with $\mathrm{Ri}_b = 0.14$, wavenumbers greater than 0.83 would be stable. Instead, a secondary maximum in σ_r is found at much higher wavenumbers ($k \sim 10^2$), where salt fingering instabilities are damped and rendered oscillatory by the shear. The latter occurs when finger amplitudes are maximized not at $z = 0$, as in the example shown in Fig. 2a, but at some other depth where the background flow is nonzero. The

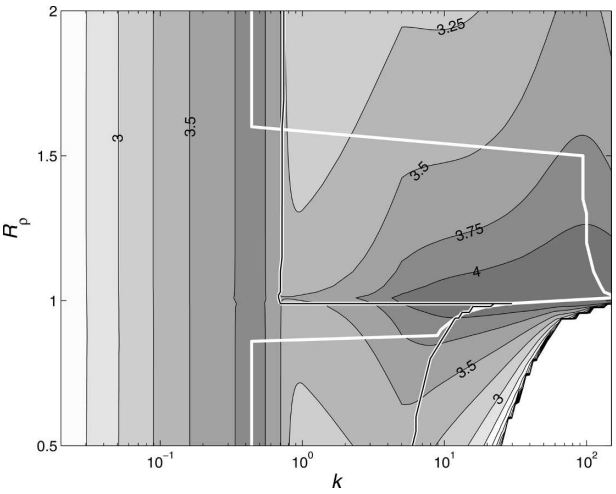

FIG. 3. Effects of double-diffusive stratification on KH instability. Shaded contours indicate $\log_{10}\sigma_r$ as a function of k and R_ρ for transverse modes ($l = 0$) with $\mathrm{Re} = 10^4$, $\mathrm{Ri}_b = 0.14$, and $\mathrm{Gr} = 10^8$. The white contour shows the wavenumber of the fastest-growing mode for each R_ρ. Modes are stationary except to the right of the black contour, where oscillatory instability occurs.

background flow therefore advects the instability, Doppler shifting the oscillation frequency away from zero. For $1 < R_\rho < 1.6$, these oscillatory salt fingers are the dominant instability.

For $0.9 < R_\rho < 1$, the dominant instability is diffusive convection. When $R_\rho < 0.9$, KH modes are again dominant and are again not significantly affected by the double-diffusive stratification (as indicated by the fact that the white curve is once again vertical).

5. How do salt sheets interact with shear?

As illustrated in Fig. lc, shear suppresses the salt fingering instability whenever the convective motions have a component in the direction of the mean flow, that is, whenever $k \neq 0$. When $k = 0$, the mean flow U no longer appears in (23)–(25), so the growth rate and the eigenfunctions $\hat{w}$, $\hat{b}_T$, and $\hat{b}_S$ are just as they would be in the absence of a mean shear (cf. Linden 1974).

In contrast, U does not vanish from the streamwise momentum equation (22), which becomes

$$(\sigma - \mathrm{Pr}\nabla^2)\hat{u} = -\hat{w}U_z. \tag{36}$$

The vertical motion of the salt sheets advects the mean shear to force a perturbation horizontal velocity. While this process does not affect the salt fingers (at the lowest order), it may have an important effect on the mean flow via the Reynolds stress $\overline{u'w'} = 2(\hat{w}^*\hat{u})_r e^{2\sigma_r t}$, in which the asterisk and the subscript r represent the complex conjugate and the real part, respectively.

We begin the discussion of salt sheets by establishing an analytical framework within which to interpret the numerical results, based on existing theories for salt fingers in an unsheared environment with uniform scalar gradients. We show that, even in a sheared environment with localized background gradients, these approximations can work very well provided Gr is sufficiently large. We then investigate the diapycnal momentum flux due to salt sheets, as described by the Schmidt number, Sc_s, the ratio of the effective viscosity of the salt sheets to their effective saline diffusivity. We find that Sc_s is much less than unity in the linear regime, indicating that salt sheets may be relatively inefficient at fluxing momentum. Last, we describe the dissipation ratio Γ, whose value is commonly used to distinguish double-diffusive mixing from mechanically driven turbulence in complex ocean environments. The linear approximation to Γ turns out to bear significant resemblance both to its finite-amplitude, steady-state form and to observational estimates.

a. Comparison with salt sheets in uniform gradients

Consider the simple case in which the aspect ratio of the salt sheets is such that the vertical derivative in $\tilde{\nabla}^2$ is negligible relative to the horizontal derivatives. This is the "tall fingers" (TF) approximation first used by Stern (1975). When $k = 0$, we may then write $\tilde{\nabla}^2 \to -l^2$. Validity of this approximation requires that the vertical scale over which salt sheet properties vary is much larger than $2\pi/l$. We express that vertical scale in dimensional terms as ch, where h is the layer thickness and c is a dimensionless scaling factor. Assuming that salt sheets can be vertically uniform only inasmuch as the mean profiles (19)–(21) are, we expect that c will be at most $O(1)$ and probably smaller. The condition for validity of the TF approximation is then, in nondimensional terms, $l \gg 2\pi/c$.

Consistent with the above assumptions, we replace the background buoyancy gradients B_{Sz} and B_{Tz}, and velocity gradient U_z, with constants equal to the gradients evaluated at $z = 0$: $B_{Tz0} = R_\rho \mathrm{GrPr}/(R_\rho - 1)$, $B_{Sz0} = -\mathrm{GrPr}/(R_\rho - 1)$, and $U_{z0} = \mathrm{RePr}$. With these assumptions, the eigenvalue problem (23)–(25) reduces to a cubic polynomial for the growth rate (Stern 1975):

$$(\sigma + \tau l^2)(\sigma + \mathrm{Pr} l^2)(\sigma + l^2) + \mathrm{GrPr}\sigma + (R_\rho \tau - 1)\frac{\mathrm{GrPr}}{R_\rho - 1} l^2 = 0. \quad (37)$$

While the TF approximation simplifies the problem considerably, it still requires the solution of a cubic poynomial.[2] To make further progress, we make the additional assumption that the growth rate is small in comparison with the viscous decay rate $\mathrm{Pr} l^2$, but large in comparison with the salinity decay rate τl^2 (Stern 1975). This formulation assumes that growth rates are purely real. We refer to this as the "viscous control" (VC) approximation. With it, the cubic is reduced to a quadratic, which is easily solved to find the growth rate and wavenumber of the fastest-growing instability:

$$\sigma = \mathrm{Gr}^{1/2} f(R_\rho), \quad f(R_\rho) = \left(\frac{R_\rho}{R_\rho - 1}\right)^{1/2} - 1, \quad (38)$$

and

$$l = \mathrm{Gr}^{1/4}. \quad (39)$$

The assumption $l \gg 2\pi/c$ now becomes $\mathrm{Gr} \gg (2\pi/c)^4 = 1559/c^4$. Given the uncertainty of c, all we can say is that Gr must be greater than $O(10^3)$, possibly by several orders of magnitude, for these approximations to be valid; however, that condition is frequently satisfied in the ocean (section 2d). The opposite extreme, $\mathrm{Gr} \ll 10^3$, corresponds to the thin interface limit, which is known to be a poor description of double-diffusive instability in the ocean (e.g., Kunze 2003).

The condition for the analytical solution in (38) and (39) to be valid, $\tau l^2 \ll \sigma \ll \mathrm{Pr} l^2$, becomes

$$\tau \ll f(R_\rho) \ll \mathrm{Pr}. \quad (40)$$

Common oceanic values of R_ρ at which salt fingering is observed range between 1.25, for which $f = 1.24$, and 3, for which $f = 0.22$. With $\tau = 0.01$ and $\mathrm{Pr} = 7$, these values are within the range specified in (40), so we may reasonably expect that the analytical solution in (38) and (39) will be relevant. In limited regions, such as certain sublayers of a thermohaline interleaving complex, R_ρ may be less than 1.25, and the resulting intense instability may not be well described by (38)–(40).

The TF approximation allows explicit solution of the buoyancy equations in (24) and (25) for longitudinal modes:

$$\hat{b}_T = \frac{-\hat{w} B_{Tz0}}{\sigma + l^2} \quad \text{and} \quad \hat{b}_S = \frac{-\hat{w} B_{Sz0}}{\sigma + \tau l^2}. \quad (41)$$

The flux ratio (34) thus becomes

$$\gamma_s = \frac{\sigma + \tau l^2}{\sigma + l^2} R_\rho, \quad (42)$$

where once again the growth rate is assumed to be real. (These results will be generalized to include complex

[2] For the complete analytic solution see Schmitt (1979, 1983).

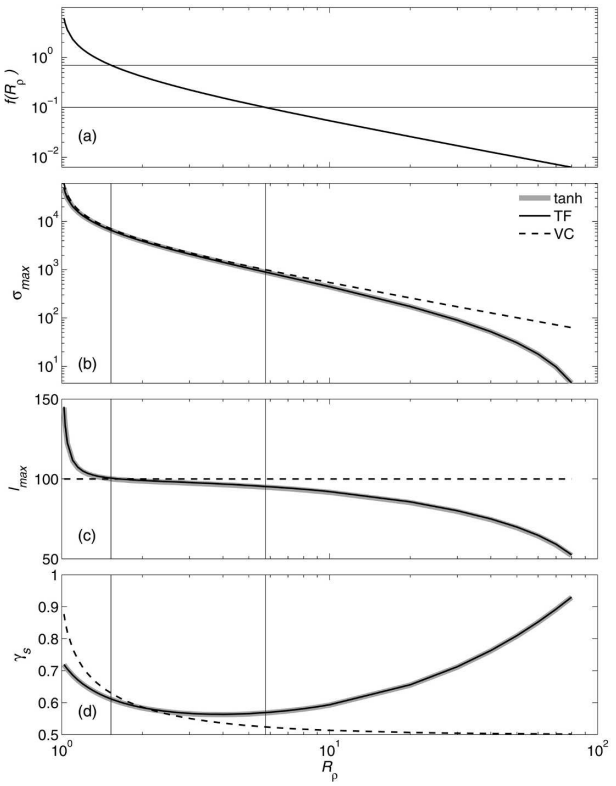

FIG. 4. Test of the TF and VC approximations for sheared, longitudinal ($k = 0$) salt sheets: $\mathrm{Gr} = 10^8$. (a) The $f(R_\rho)$, (b) FGM growth rate, (c) FGM spanwise wavenumber, and (d) flux ratio vs density ratio. Straight lines correspond to $f = 10\tau$, $f = \mathrm{Pr}/10$, the approximate limits for the validity of the VC approximation. Thick, shaded curves show numerically computed results for the hyperbolic tangent profiles in (26)–(28).

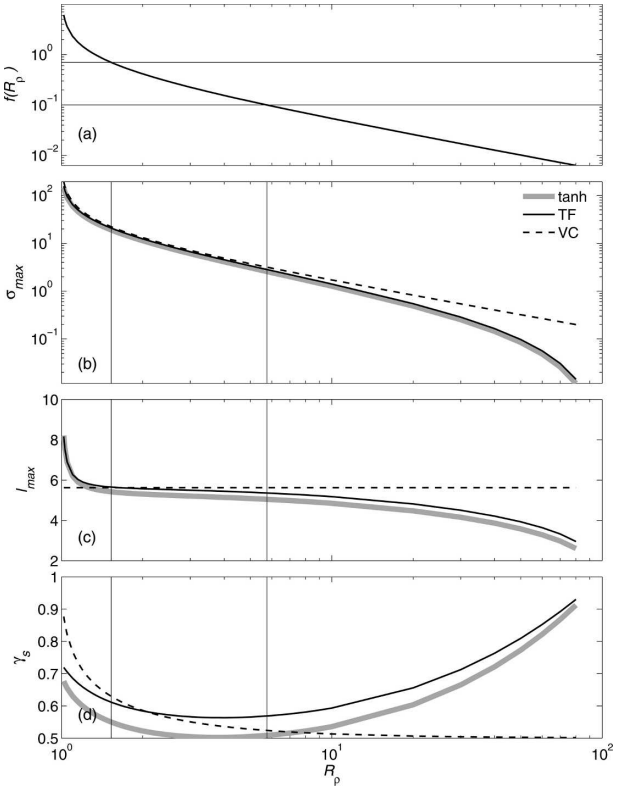

FIG. 5. Same as in Fig. 4, but for $\mathrm{Gr} = 10^3$.

growth rates in section 6.) We cannot evaluate γ_s explicitly without knowledge of σ and l, but we can deduce the bounds $R_\rho\tau \le \gamma_s < R_\rho$. The VC approximation now allows us to substitute from (38) and (39) to obtain

$$\gamma_s = R_\rho^{1/2}[R_\rho^{1/2} - (R_\rho - 1)^{1/2}] \tag{43}$$

(e.g., Stern 1975; Kunze 2003).

Equivalent results for the localized gradients considered in this paper are obtained numerically and are then compared with the theoretical results for uniform gradients reviewed above. In Fig. 4, we show results for a case in which $\mathrm{Gr} = 10^8$. This Grashof number is at the low end of the observed range; nevertheless, it exceeds 10^3 by five orders of magnitude, so we anticipate that the TF approximation will work well. The TF approximation predicts growth rates (Fig. 4b), wavenumbers (Fig. 4c), and flux ratios (Fig. 4d) of salt sheet instabilities accurately over the entire range of R_ρ. In particular the nonmonotonic dependence of γ_s on R_ρ that leads to staircase formation in the model of Radko (2003) is reproduced. Not surprisingly, the VC approximation is less successful. It gives useful results for a limited range of R_ρ in which (40) is valid (Fig. 4a).

When the Grashof number is reduced to 10^3, the TF approximation becomes marginally accurate (Fig. 5). Growth rates, wavenumbers, and flux ratios are all overpredicted, typically by a few percent.

b. The Schmidt number

Results quoted so far are independent of the mean flow. We turn now to the momentum flux driven by salt sheets aligned with the mean flow so that $k = 0$. The streamwise momentum Eq. (36) may be solved and multiplied by $\hat{w}^*$ to obtain

$$\overline{u'w'} = \frac{-2|\hat{w}|^2 U_{z0}}{\sigma + \mathrm{Pr}l^2}\, e^{2\sigma_r t}. \tag{44}$$

This specific momentum flux may be expressed in terms of a salt sheet viscosity ν_s that is independent of the mean flow:

$$\nu_s \equiv \frac{-\overline{u'w'}}{U_z} = \frac{2|\hat{w}|^2}{\sigma + \mathrm{Pr}l^2}\, e^{2\sigma_r t}. \tag{45}$$

Recall that all quantities on the right-hand side of (45) are independent of U when $k = 0$. Thus, (45) may be combined with the saline diffusivity derived in the same manner from (41) to form the effective Schmidt number:

$$\mathrm{Sc}_s \equiv \frac{-\overline{u'w'}/U_z}{-\overline{b'_S w'}/B_{Sz}} = \frac{\sigma + \tau l^2}{\sigma + \mathrm{Pr} l^2}. \tag{46}$$

This Schmidt number provides a useful route to estimation of the eddy viscosity of salt fingers via the more easily measured saline diffusivity. As a ratio of fluxes, it is independent of time, so that an estimate based on linear theory may be relevant at finite amplitude. Equation (46) shows that, in the TF approximation, Sc_s is also independent of the background shear and is bounded by $\mathrm{Sc}^{-1} \le \mathrm{Sc}_s < 1$. Recall that Sc is the molecular Schmidt number, equal to 700 in this study. The limiting case $\sigma = 0$, for which Sc_s takes its lower bound, Sc^{-1}, was described by Ruddick (1985). Note that the lower bound is positive, so that negative eddy viscosities are excluded. The upper bound $\mathrm{Sc}_s < 1$ shows that eddy viscosity cannot exceed saline diffusivity.

Doing the same with the thermal buoyancy yields a Prandtl number that has similar form and is bounded by $\mathrm{Pr}^{-1} < \mathrm{Pr}_{\mathrm{sf}} < 1$. We focus on the Schmidt number here, because saline buoyancy is the force that drives salt sheets. If the Prandtl number is needed, it is readily obtained as $\mathrm{Pr}_s = \mathrm{Sc}_s R_\rho / \gamma_s$.

If, in addition, we now make the VC assumption (40), the Schmidt number becomes

$$\mathrm{Sc}_s = \frac{f(R_\rho)}{\mathrm{Pr}}. \tag{47}$$

The Schmidt number is now independent not only of the mean shear but also of Gr. For a given Pr, the Schmidt number depends only on R_ρ.

Again, equivalent results for the case of localized gradients must be obtained numerically. Based on (46) and (47), we may anticipate that, at sufficiently high Gr, the salt sheet Schmidt number will be, first, approximately independent of the mean flow and, second, bounded approximately within the interval $(\mathrm{Sc}^{-1}, 1)$. Moreover, when (40) holds, Sc_s will depend only on R_ρ and Pr in accordance with (47).

Numerical results for localized gradients with shear are shown in Fig. 6. We have chosen one case with $\mathrm{Gr} \gg 10^3$, so that TF is expected to be accurate, plus two cases at smaller Gr where a dependence on the mean shear is possible. We focus on the range $1 < R_\rho \le 4$, where salt sheet growth rates are significant.

At $\mathrm{Gr} = 10^8$ (Fig. 6a), the TF approximation is highly accurate. A particular consequence of TF that is confirmed in Fig. 6a is the bound $\mathrm{Sc}^{-1} < \mathrm{Sc}_s < 1$. (Note that $\mathrm{Sc}^{-1} = 1.4 \times 10^{-3}$, which is off the scale.) The VC is much less accurate, overpredicting the Schmidt number significantly in a range of small but oceanographically important values of R_ρ.

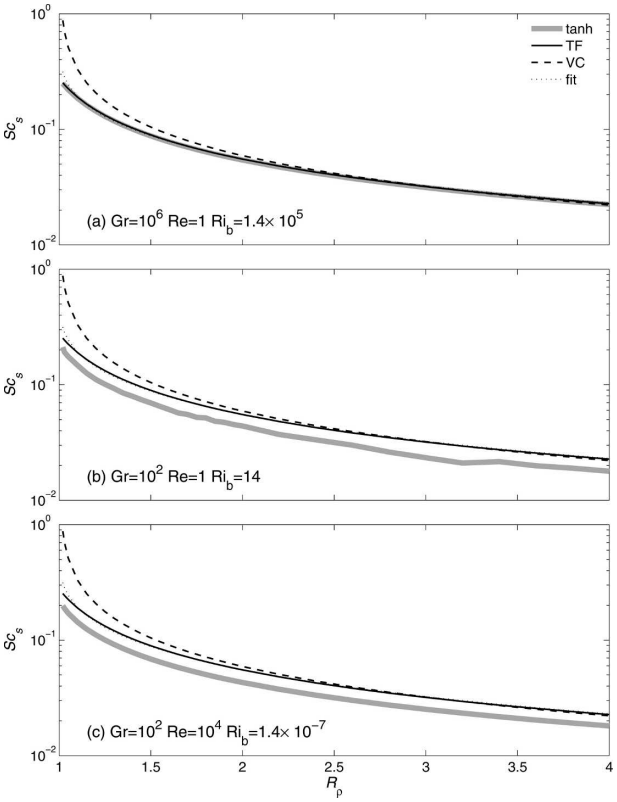

FIG. 6. Schmidt number vs density ratio for sheared, longitudinal salt sheets. The TF, VC, and empirical [(48)] approximations are identified in the legend in (a). (a) TF is valid at high Gr. (b), (c) Even at low Gr, the Schmidt number is essentially independent of the mean shear.

Unlike the mode properties considered in section 5a, the Schmidt number is not guaranteed to be independent of the background shear by Squire's theorem. That independence is a consequence of the TF approximation, and may therefore fail if Gr is not $\gg 10^3$, as is the case in Figs. 6b,c. These examples have very weak shear ($\mathrm{Re} = 1$; $\mathrm{Ri}_b = 14$) and very strong shear ($\mathrm{Re} = 10^4$; $\mathrm{Ri}_b = 1.4 \times 10^{-7}$), respectively. In both cases the TF approximation overpredicts Sc_s by a few tens of percent. Note that there is no significant difference between the weakly and strongly sheared cases. Although the TF approximation that makes mean shear irrelevant is not valid for these cases, the mean shear has no discernible effect.

Because the VC approximation (47) is invalid at low R_ρ, we propose an empirical fit for the Schmidt number:

$$\mathrm{Sc}_s = 0.08 \ln\left(\frac{R_\rho}{R_\rho - 1}\right). \tag{48}$$

This is shown by the dotted curves on Fig. 6. Equation (48) is a good fit to the TF approximation to Sc_s, and is therefore valid wherever the latter is. Our previous scaling considerations led to the criterion $\mathrm{Gr} \gg 10^3$, while numerical results suggest that $\mathrm{Gr} > 10^4$ is sufficient. This condition is commonly satisfied in the ocean; for example, in the Barbados observations $10^8 \leq \mathrm{Gr} \leq 2 \times 10^9$ (section 2b), exceeding the requirement by at least four orders of magnitude. The fit in (48) shows significant deviations from the numerical result only at extremely low values of R_ρ. The latter can be remedied by capping Sc_s at 0.3 for $R_\rho < 1.02$.

c. The dissipation ratio

The dissipation ratio Γ (Oakey 1985) is frequently used as a surrogate for mixing efficiency in observational data analysis (e.g., Moum 1996; Ruddick et al. 1997; Smyth et al. 2001), and also for distinguishing mixing due to salt fingering from that due to shear-driven turbulence (e.g., McDougall and Ruddick 1992; St. Laurent and Schmitt 1999). The dissipation ratio may be defined in terms of either temperature or salinity, but the former is used more commonly for ease of measurement:

$$\Gamma = \frac{\chi B_z}{2\varepsilon B_{Tz}^2}. \tag{49}$$

Here, χ represents the dissipation rate of thermal buoyancy variance, $\chi = \langle 2|\nabla b_T|^2\rangle$ in nondimensional form, and $\varepsilon = \langle 2\mathrm{Pr}\, e_{ij}^2\rangle$ is the dissipation rate of perturbation kinetic energy. The tensor $e_{ij} = (\partial u_i/\partial x_j + \partial u_j/\partial x_i)/2$ represents the strain rate. Angle brackets indicate a spatial average, over the wavelength of the disturbance in the present context.

At steady state, balances of kinetic energy and scalar variance imply

$$\Gamma = \frac{R_f}{R_f - 1}\frac{R_\rho - 1}{R_\rho}\frac{\gamma_s}{1 - \gamma_s}, \tag{50}$$

where $R_f = -\overline{(b_T' + b_S')w'}/\overline{u'w'}\, U_z$ is the flux Richardson number (St. Laurent and Schmitt 1999). For unsheared salt fingers, this takes the simpler form:

$$\Gamma = \frac{R_\rho - 1}{R_\rho}\frac{\gamma_s}{1 - \gamma_s} \tag{51}$$

(Hamilton et al. 1989; McDougall and Ruddick 1992).

Shear-driven turbulence typically gives values of Γ near 0.2 (Moum 1996), whereas higher values are expected for salt fingers. St. Laurent and Schmitt (1999) found Γ ranging up to 0.6, and occasionally higher, in regions of strong thermal microstructure but weak shear, and concluded that the microstructure was due to salt fingering.

In the linear regime of interest to us here, both χ and ε grow exponentially in time, but their ratio is constant, so that the value of Γ may conceivably have some relevance for finite-amplitude disturbances. Applying the TF approximation for longitudinal salt sheets [i.e. setting $k = 0$, $\hat{v} = 0$, and $\partial/\partial z = 0$, solving for $\hat{u}$ and $\hat{b}_T$ as was done in section 5b, and substituting into (49)], one obtains

$$\Gamma_{\mathrm{TF}} = \frac{\mathrm{Gr}}{(\sigma + l^2)^2}\frac{(\sigma + \mathrm{Pr}l^2)^2}{\mathrm{Re}^2\mathrm{Pr}^2 + (\sigma + \mathrm{Pr}l^2)^2}. \tag{52}$$

In contrast to the Schmidt number, Γ is clearly a function of the mean shear (via Re) in the TF approximation. This is because perturbation velocities parallel to U (which are orthogonal to the salt sheet motions and do not affect their behavior in any way) make a significant contribution to ε.

The TF approximation in (52) can be shown to be bounded by $0 \leq \Gamma_{\mathrm{TF}} \leq \mathrm{Gr}/(\mathrm{Re}^2 + l^4)$. The upper bound corresponds to the steady state $\sigma = 0$. As a consistency check, one may set $\sigma = 0$ in (37), (42), (46), and (52) and combine to reproduce the finite-amplitude, steady-state result in (50).

When the VC approximation is made, (52) becomes

$$\Gamma_{\mathrm{VC}} = \frac{R_\rho - 1}{R_\rho}\frac{\mathrm{Gr}}{\mathrm{Gr} + \mathrm{Re}^2} = \frac{R_\rho - 1}{R_\rho}\frac{\mathrm{PrRi}_b}{\mathrm{PrRi}_b + 1}. \tag{53}$$

Note that the dependence on R_ρ is the same as in the steady-state case (50), but other details differ. As is clearest from the first equality in (53), the imposition of shear ($\mathrm{Re} > 0$) acts to reduce Γ_{VC}. The second equality shows that shear effects are negligible when $\mathrm{Ri}_b \gg \mathrm{Pr}^{-1}$, whereas shear effects dominate when $\mathrm{Ri}_b \ll \mathrm{Pr}^{-1}$ and take Γ_{VC} to zero in the limit $\mathrm{Ri}_b \to 0$. In that case, the salt sheets are supplanted by shear instability. The latter class of modes, being transverse, is not described by (53), but typically has $\Gamma \sim 0.2$ or less.[3] For example, the shear instability shown in Figs. 2b,c has $\Gamma = 0.174$.

Results for the fastest-growing salt sheet instability with $\mathrm{Gr} = 10^8$ are shown in Fig. 7. Here R_ρ is set to the oceanographically common value of 2. The TF approximation is accurate to within 1% of the numerical value for a wide range *of* Ri_b, while the VC approximation is up to ~10% low. For $\mathrm{Ri}_b < 0.08$, Γ is smaller than 0.2, the canonical value for shear-driven turbulence.

[3] Note that significantly higher values are possible for preturbulent, finite-amplitude KH billows (e.g., Smyth et al. 2001).

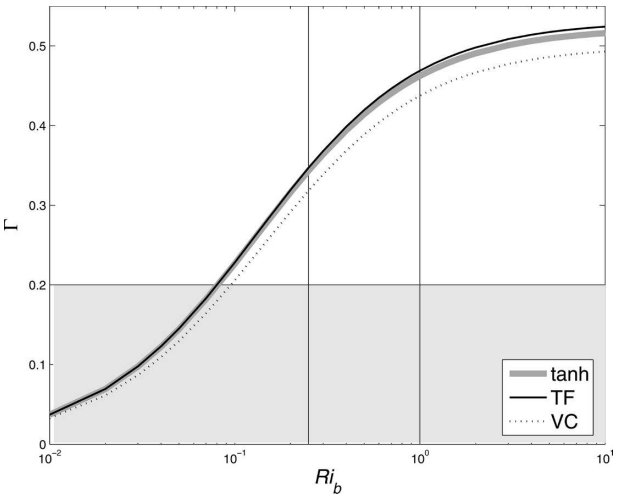

FIG. 7. Dissipation ratio vs minimum Richardson number for salt sheets with $R_\rho = 2$, $\mathrm{Gr} = 10^8$, and $k = 0$. Solid and dotted curves show the TF and VC approximations. The shaded region represents the range $0 < \Gamma \leq 0.2$ expected for shear-driven turbulence. Vertical lines indicate $\mathrm{Ri}_b = 0.25$ and $\mathrm{Ri}_b = 1$.

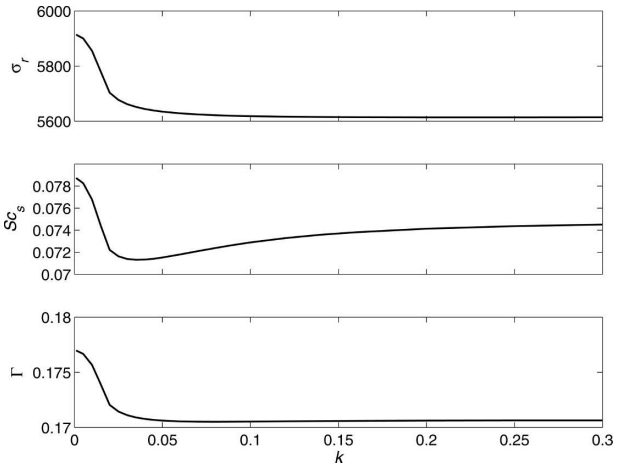

FIG. 8. (a) Real growth rate, (b) Schmidt number, and (c) dissipation ratio vs wavenumber k, for salt fingers with $\mathrm{Gr} = 10^8$, $\mathrm{Ri}_b = 0.1$, $\mathrm{Re} = 10^4$, and $l = 99.8$.

At large Ri_b (weak shear), Γ asymptotes to a value slightly higher than than the VC limit $(R_\rho - 1)/R_\rho = 0.5$. This is consistent with values observed at high Richardson number by St. Laurent and Schmitt (1999, their Fig. 9), although the increase in Γ at high Ri is greater in the observations. The observed dependence of Γ on R_ρ is opposite to the theoretical prediction, showing a decrease with increasing R_ρ where all theories [(50), (51), (52), (53)] predict an increase.

In the linear case, shear effects become dominant when $\mathrm{Ri}_b < \mathrm{Pr}^{-1} = 1/7$, whereas in the observations the change in Γ occurs near $\mathrm{Ri} = 1$. This discrepancy reflects the approximations inherent in linear theory, but it is also due in part to a difference in the definition of the Richardson number. Here, Ri_b is the minimum value of the gradient Richardson number, evaluated precisely at the center of the shear layer. In contrast, the observational Ri is based on the shear of a velocity profile measured with ~1-m resolution. Averaging inevitably smoothes away some fraction of the shear and thus leads to higher Ri.

We conclude that the behavior of the salt sheet dissipation ratio in the linear regime is relevant at finite amplitude. In particular, the known tendency of shear to reduce Γ is manifest in small-amplitude salt sheets.

d. Obliquity effects

Longitudinal salt sheets have $k = 0$ and are therefore not directly affected by the mean shear $U(z)$. When k becomes nonzero, the mean flow acts to damp the growth rate, as shown on Fig. 1c. The possibility exists, however, that these *oblique* salt finger modes could interact with the mean shear in other ways, possibly generating a strong momentum flux, and/or rapid kinetic energy dissipation, despite their relatively low growth rates. In an environment with fluctuating shear (e.g., inertial oscillations) salt sheets are always at least slightly oblique, and hence have the potential to interact with the mean shear in unexpected ways.

Figure 8 shows the k dependence of the growth rate, Schmidt number, and dissipation ratio for a case with realistic Grashof number and strong shear ($\mathrm{Ri}_b = 0.1$). The result is essentially negative. Increasing k from zero causes a small decrease in the growth rate, but differences in Sc_s and Γ are insignificant. In conclusion, obliquity does not appear to alter the conclusions previously drawn in this section.

6. How does diffusive convection interact with shear?

The VC approximation is invalid in the diffusive convection regime because σ_i is generally not $\ll \mathrm{Pr}l^2$. We will, however, extend the TF approximation to obtain a Prandtl number for diffusive convection in a shear flow. [Because thermal buoyancy is the driving force behind diffusive convection, flux parameterizations are generally expressed in terms of a thermal diffusivity and a Prandtl number (e.g., Walsh and Ruddick 1998). If needed, the Schmidt number can be computed as $\mathrm{Sc}_d = \mathrm{Pr}_d R_\rho/\gamma_d$.] We simply extend (44)–(46) to allow for complex growth rates, and replace saline buoyancy with thermal buoyancy. The result is

$$\mathrm{Pr}_d \equiv \frac{-\overline{u'w'}/U_z}{-\overline{b'_T w'}/B_{Tz}} = \frac{[1/(\sigma + \mathrm{Pr}l^2)]_r}{[1/(\sigma + l^2)]_r}. \qquad (54)$$

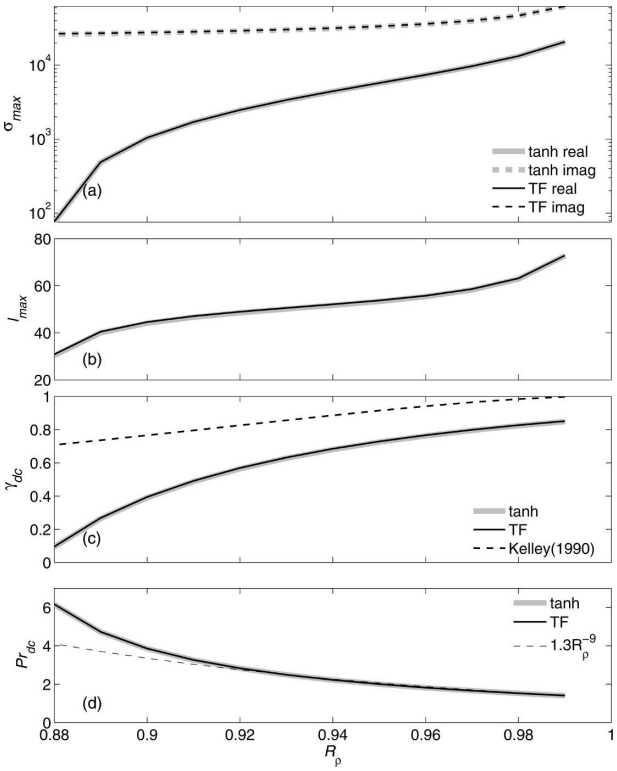

FIG. 9. Test of the TF approximation for weakly sheared diffusive convection cells. Gr = 10^8; Re = 10^4. (a) FGM growth rate, (b) spanwise wavenumber, (c) flux ratio, and (d) Prandtl number vs density ratio. Also shown in (c) is the flux ratio for diffusive convection in the laboratory (Kelley 1990). Also shown in (d) is an empirical fit $\mathrm{Pr}_d = 1.3R_\rho^{-9}$.

The addition of oscillatory modes expands the range of possible Prantdl numbers from $\mathrm{Pr}^{-1} < \mathrm{Pr}_s < 1$ (found in the salt fingering case) to $\mathrm{Pr}^{-1} < \mathrm{Pr}_d < \mathrm{Pr}$ (i.e., the TF approximation leads us to expect that the Prandtl number for diffusive convection may be greater than unity).

The truth of this prediction is demonstrated in Fig. 9, which shows a case with relatively strong double-diffusive instability (Gr = 10^8) and shear (Re = 10^4). The TF approximation predicts growth rates, oscillation frequencies, and wavenumbers very accurately in this case (Figs. 9a,b). Also well predicted are the flux ratio and the Prandtl number. The flux ratio is somewhat smaller than the laboratory-based empirical formulation of Kelley (1990). We take this discrepancy as a caution that finite-amplitude diffusive convection may not be well modeled by its linear counterpart. The Prandtl number Pr_d increases from 1.2 in the limit $R_\rho \to 1^-$ to higher values at lower R_ρ. This result is also consistent with Padman (1994), who obtained $1 < \mathrm{Pr}_d < 3$ from observations of a thermohaline staircase in the Arctic.

To approximate the dependence of the diffusive convection Prandtl number on R_ρ, we recommend the empirical fit:

$$\mathrm{Pr}_d = \begin{cases} 1.3R_\rho^{-9}, & \text{if} \quad 0.9 < R_\rho < 1 \\ 3.4, & \text{if} \quad 0 < R_\rho < 0.9 \end{cases}. \tag{55}$$

This fit is generally good to within 10%, better at $R_\rho \approx 1$, where diffusive convection is strong. The exponential fit is terminated at $R_\rho = 0.9$ to prevent the overprediction of momentum fluxes at lower R_ρ, where diffusive convection is inactive according to linear theory but not according to laboratory experiments (Kelley 1990).

We do not investigate the dissipation ratio Γ in detail for the diffusive convection case since the VC approximation is not available for comparison, but we note that numerically computed values are generally much smaller than those computed for salt sheets. Typical values are $O(0.1)$ at high Ri_b, and drop to zero in strong shear as was found for salt sheets. The sheared diffusive convection example shown in Figs. 2f,g has $\Gamma = 0.024$.

7. Which mode dominates?

For oceanic parameter values, the KH growth rate may be approximated by a linear fit to the numerical results of Hazel (1972), nondimensionalized as described in section 2a:

$$\sigma_{\mathrm{KH}} = 0.2\mathrm{RePr}(1 - 4\mathrm{Ri}_b). \tag{56}$$

Equating this with the salt sheet growth rate given by (38), we obtain

$$0.2\mathrm{Pr}^{1/2}(1 - 4\mathrm{Ri}_b)\mathrm{Ri}_b^{-1/2} = f(R_\rho), \tag{57}$$

which for any given Pr describes a curve on the $\mathrm{Ri}_b - R_\rho$ plane upon which the growth rates of the fastest-growing KH and salt sheet modes are equal. For a given R_ρ, (57) is easily solved for Ri_c, the critical Richardson number above which salt sheet instability dominates.

Explicit calculation for the localized profiles (Fig. 10) confirms that Ri_c based on (57) is accurate to within 10%. The growth rates of KH and double-diffusive instabilities are comparable throughout the region where the individual instabilities are significant, and the double-diffusive growth rate exceeds the KH growth rate over much of this region. We conclude that, even in the presence of inflectional shear with $\mathrm{Ri}_b < \frac{1}{4}$, double-diffusive instabilities are likely to play an important role.

8. Conclusions

We have computed the linear stability characteristics of a stratified shear layer in which the stratification

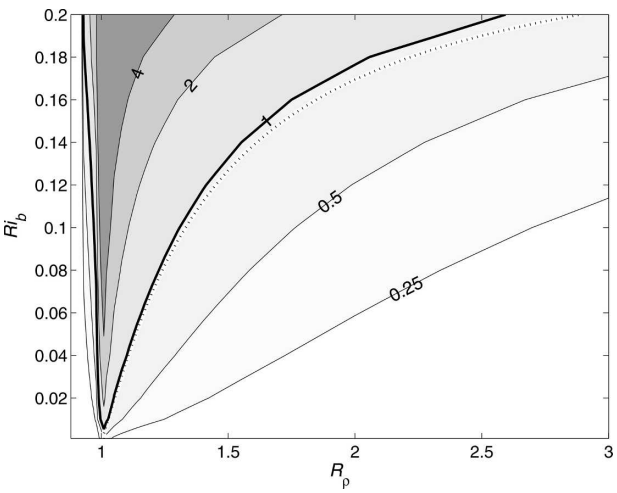

FIG. 10. Ratio of double-diffusive growth rate to KH growth rate for Gr = 108, Pr = 7. The dotted line is the analytical approximation in (57).

supports double-diffusive instabilities, and compared the results with the existing understanding of inflectional shear instabilities, salt fingering, and diffusive convection in uniform gradients. An important goal has been to parameterize momentum fluxes driven by double-diffusive instabilities. Our main findings are as follows:

- The finite thickness of the stratified layer has a significant effect on the double-diffusive modes only when $\mathrm{Gr} < 10^4$. For the larger values typical of oceanic double diffusion, stability characteristics are predicted accurately by the "tall fingers" approximation, which assumes that background gradients are uniform.
- Even in the presence of inflectional shear with $\mathrm{Ri}_b < \frac{1}{4}$, double-diffusive instabilities are strong enough to play an important role in the dynamics. In the salt-fingering regime, the surface on which the growth rates are equal is given approximately by (57).
- Properties of the linear KH instability are affected negligibly by diffusively unstable stratification unless R_ρ is close to unity.
- Momentum flux by salt sheets is described by a Schmidt number Sc_s which lies in the range $\mathrm{Sc}^{-1} < \mathrm{Sc}_s < 1$ and is by and large much smaller than unity. Here Sc_s is determined primarily by R_ρ. For oceanically relevant parameter values, the parameterization in (48) provides an accurate estimate of Sc_s. The result $\mathrm{Sc}_s < 1$ suggests that fingering layers are less viscous than is commonly assumed. This has important implications for thermohaline interleaving in the fingering regime, where initial growth is governed largely by momentum fluxes due to salt sheets (Walsh and Ruddick 1998; Mueller et al. 2007).
- Negative eddy viscosity, via which salt fingers amplify the mean shear (e.g., Stern 1969; Paparella and Spiegel 1999; Stern and Simeonov 2005), is not found in these calculations. For localized shear and stratification, the cases computed here have given uniformly positive eddy viscosity (or, equivalently, $\mathrm{Sc}_s > 0$). For salt sheets in the TF approximation, we have given a general proof that Sc_s is bounded from below by Sc^{-1}, which is positive. There is no inconsistency in this result, as it is the primary instability we compute, whereas negative eddy viscosity results from a secondary instability involving the collective deformation of several wavelengths of the primary mode. Also, we have focused on salt sheets, which cannot be affected by the mean flow in the small-amplitude limit.
- Momentum flux by diffusive convection cells is described by a Prandtl number Pr_d such that $\mathrm{Pr}^{-1} < \mathrm{Pr}_d < \mathrm{Pr}$. Here Pr_d is determined primarily by R_ρ and is generally greater than unity. For oceanically relevant parameter values, the parameterization in (55) provides a plausible estimate of Pr_d. In contrast to the result for salt sheets, $\mathrm{Pr}_d > 1$ suggests that interleaving in diffusive regimes (e.g., the polar oceans) grows relatively slowly. While linear theory is questionable as a description of diffusive convection, the result $\mathrm{Pr}_d > 1$ is supported by observations (Padman 1994).
- The dissipation ratio Γ can be meaningfully predicted from linear theory, and agrees well with both observations and predictions based on a finite-amplitude, production–dissipation balance.

These results are now being used in the modeling of thermohaline interleaving, where the possibility that $\mathrm{Sc}_s < 1$ and $\mathrm{Pr}_d > 1$ have significant implications for intrusion growth and equilibration (e.g., Mueller et al. 2007). The next stages in this line of research will involve 1) an extension to more general background profiles, and 2) moving beyond linear perturbation theory and into the fully turbulent regime via direct numerical simulations. There, it is expected that salt sheets will interact with the secondary instability of KH billows (e.g., Klaassen and Peltier 1991), which are also longitudinal in form. These simulations will allow us to test rigorously the momentum flux parameterizations suggested in the present linear analyses.

Acknowledgments. This project has benefited from discussions with Rachael Mueller. We also appreciate thoughtful critiques by Eric Kunze, Ray Schmitt, and

an anonymous reviewer. Rita Brown provided editorial assistance. The work was supported by the National Science Foundation under Grants OCE0095640 (W. D. Smyth) and OCE0453140 (S. Kimura).

REFERENCES

Baines, P., and A. Gill, 1969: On thermohaline convection with linear gradients. *J. Fluid Mech.,* **34,** 289–306.

Deardorff, J., 1965: Gravitational instability between horizontal plates with shear. *Phys. Fluids,* **8A,** 1027–1030.

Gregg, M. C., and T. Sanford, 1987: Shear and turbulence in thermohaline staircases. *Deep-Sea Res.,* **34,** 1689–1696.

Hamilton, J., M. Lewis, and B. Ruddick, 1989: Vertical fluxes of nitrate associated with salt fingers in the world's oceans. *J. Geophys. Res.,* **94,** 2137–2145.

Hazel, P., 1972: Numerical studies of the stability of inviscid parallel shear flows. *J. Fluid Mech.,* **51,** 39–62.

Hebert, D., 1988: Estimates of salt-finger fluxes. *Deep-Sea Res.,* **35,** 1887–1901.

Holyer, J., 1981: On the collective instability of salt fingers. *J. Fluid Mech.,* **110,** 195–207.

Howard, L., 1961: Note on a paper of John W. Miles. *J. Fluid Mech.,* **10,** 509–512.

Kelley, D., 1990: Fluxes through diffusive staircases: A new formulation. *J. Geophys. Res.,* **95,** 3365–3371.

Klaassen, G., and W. Peltier, 1991: The influence of stratification on secondary instability in free shear layers. *J. Fluid Mech.,* **227,** 71–106.

Kunze, E., 1990: Limits on growing, finite-length salt fingers: A Richardson number constraint. *J. Mar. Res.,* **45,** 533–556.

——, 1994: A proposed flux constraint for salt fingers in shear. *J. Mar. Res.,* **52,** 999–1016.

——, 2003: A review of oceanic salt fingering theory. *Progress in Oceanography,* Vol. 56, Pergamon Press, 399–417.

Lee, V., and C. Caulfield, 2001: Nonlinear evolution of a layered stratified shear flow. *Dyn. Atmos. Oceans,* **34,** 103–124.

Linden, P., 1974: Salt fingers in a steady shear flow. *Geophys. Fluid Dyn.,* **6,** 1–27.

McDougall, T., and B. Ruddick, 1992: The use of ocean microstructure to quantify both turbulent mixing and salt fingering. *Deep-Sea Res.,* **39,** 1931–1952.

Merryfield, W. J., 2000: Origin of thermohaline staircases. *J. Phys. Oceanogr.,* **30,** 1046–1068.

——, G. Holloway, and A. E. Gargett, 1999: A global ocean model with double-diffusive mixing. *J. Phys. Oceanogr.,* **29,** 1124–1142.

Miles, J., 1961: On the stability of heterogeneous shear flows. *J. Fluid Mech.,* **10,** 496–508.

Moum, J., 1996: Efficiency of mixing in the main thermocline. *J. Geophys. Res.,* **101** (C5), 12 057–12 069.

Mueller, R. D., W. D. Smyth, and B. R. Ruddick, 2007: Shear and convective turbulence in a model of thermohaline intrusions. *J. Phys. Oceanogr.,* in press.

Oakey, N., 1985: Statistics of mixing parameters in the upper ocean during JASIN phase 2. *J. Phys. Oceanogr.,* **15,** 1662–1675.

Padman, L., 1994: Momentum fluxes through sheared oceanic thermohaline steps. *J. Geophys. Res.,* **99,** 22 491–22 499.

——, and T. M. Dillon, 1987: Vertical heat fluxes through the Beaufort Sea thermohaline staircase. *J. Geophys. Res.,* **92,** 10 799–10 806.

Paparella, F., and E. Spiegel, 1999: Sheared salt fingers: Instability in a truncated system. *Phys. Fluids,* **11A,** 1161–1168.

Radko, T., 2003: A mechanism for layer formation in a double diffusive fluid. *J. Fluid Mech.,* **497,** 365–380.

Ruddick, B., 1985: Momentum transport in thermohaline staircases. *J. Geophys. Res.,* **90,** 895–902.

——, T. McDougall, and J. Turner, 1989: The formation of layers in a uniformly stirred density gradient. *Deep-Sea Res.,* **36,** 579–609.

——, D. Walsh, and N. Oakey, 1997: Variations in apparent mixing efficiency in the North Atlantic Central Water. *J. Phys. Oceanogr.,* **27,** 2589–2605.

Rudels, B., G. Bjork, R. Muench, and U. Schauer, 1999: Double diffusive layering in the Eurasian Basin of the Arctic Ocean. *J. Mar. Syst.,* **21,** 3–27.

Schmitt, R. W., 1979: The growth rate of super-critical salt fingers. *Deep-Sea Res.,* **26A,** 23–44.

——, 1983: The characteristics of salt fingers in a variety of fluid systems, including stellar interiors, liquid metals, oceans, and magmas. *Phys. Fluids,* **26A,** 2373–2377.

——, 1994: Triangular and asymmetric salt fingers. *J. Phys. Oceanogr.,* **24,** 855–860.

——, 2003: Observational and laboratory insights into salt finger convection. *Progress in Oceanography,* Vol. 56, Pergamon Press, 419–433.

Smyth, W. D., and K. B. Winters, 2003: Turbulence and mixing in Holmboe waves. *J. Phys. Oceanogr.,* **33,** 694–711.

——, J. N. Moum, and D. R. Caldwell, 2001: The efficiency of mixing in turbulent patches: Inferences from direct simulations and microstructure observations. *J. Phys. Oceanogr.,* **31,** 1969–1992.

Stern, M., 1960: The salt fountain and thermohaline convection. *Tellus,* **12,** 172–175.

——, 1969: Collective instability of salt fingers. *J. Fluid Mech.,* **35,** 209–218.

——, 1975: *Ocean Circulation Physics.* Academic Press, 246 pp.

——, and J. Simeonov, 2005: The secondary instability of salt fingers. *J. Fluid Mech.,* **533,** 361–380.

St. Laurent, L., and R. W. Schmitt, 1999: The contribution of salt fingers to vertical mixing in the North Atlantic Tracer Release Experiment. *J. Phys. Oceanogr.,* **29,** 1404–1424.

Thangham, S., A. Zebib, and C. Chen, 1984: Salt finger convection in shear flow. *Phys. Fluids,* **27A,** 804–811.

Timmermans, M.-L., C. Garrett, and E. Carmack, 2003: The thermohaline structure and evolution of the deep waters in the Canada Basin, Arctic Ocean. *Deep-Sea Res.,* **50,** 1305–1321.

Toole, J. M., and D. T. Georgi, 1981: On the dynamics and effects of double diffusive intrusions. *Progress in Oceanography*. Vol. 10, Pergamon Press, 121–145.

Walsh, D., and B. Ruddick, 1998: Nonlinear equilibration of thermohaline intrusions. *J. Phys. Oceanogr.,* **28,** 1043–1069.

Wells, M., R. Griffiths, and J. Turner, 2001: Generation of density fine structure by salt fingers in a spatially periodic shear. *J. Geophys. Res.,* **106,** 7027–7036.

Yih, C.-S., 1955: Stability of two-dimensional parallel flows for three-dimensional disturbances. *Quart. Appl. Math.,* **12,** 434–435.

You, Y., 2002: A global ocean climatological atlas of the Turner angle: Implications for double diffusion and watermass structure. *Deep-Sea Res.,* **49,** 2075–2093.

Zhang, J., R. W. Schmitt, and R. X. Huang, 1998: Sensitivity of the GFDL modular ocean model to parameterization of double-diffusive processes. *J. Phys. Oceanogr.,* **28,** 589–605.